

See discussions, stats, and author profiles for this publication at: <https://www.researchgate.net/publication/49668347>

Solid-State Reactions in Binary Molecular Assemblies of F16CuPc and Pentacene

ARTICLE *in* ACS NANO · JANUARY 2011

Impact Factor: 12.88 · DOI: 10.1021/nm102887x · Source: PubMed

CITATIONS

22

READS

38

4 AUTHORS, INCLUDING:



[Yutaka Wakayama](#)

National Institute for Materials Science

149 PUBLICATIONS 1,874 CITATIONS

[SEE PROFILE](#)



[Dimas G de Oteyza](#)

Donostia International Physics Center

60 PUBLICATIONS 1,079 CITATIONS

[SEE PROFILE](#)



[Duncan J. Mowbray](#)

Universidad del País Vasco / Euskal Herrik...

77 PUBLICATIONS 1,084 CITATIONS

[SEE PROFILE](#)

Solid-State Reactions in Binary Molecular Assemblies of F₁₆CuPc and Pentacene

Yutaka Wakayama,^{*,†,‡} Dimas G. de Oteyza,^{†,§} Juan M. Garcia-Lastra,[†] and Duncan J. Mowbray^{§,†}

[†]Advanced Electronic Materials Center, National Institute for Materials Science, 1-1 Namiki, Tsukuba 305-0044, Japan, [‡]Department of Chemistry and Biochemistry, Faculty of Engineering, Kyushu University, 1-1 Namiki, Tsukuba 305-0044, Japan, [§]Donostia International Physics Center, Paseo Manuel Lardizabal 4, San Sebastián, Spain, and [†]Nano-Bio Spectroscopy Group and European Theoretical Spectroscopy Facility, Departamento Física de Materiales UPV/EHU, Apartado 1072, San Sebastián, Spain

What are the origins of the various semiconductor functionalities? Silicon, which is a typical semiconductor, is simply a black inorganic material that has no intrinsic functionality. However, a great advantage of Si is that it can be blended with heterogeneous materials. For example, a Si matrix can be doped with impurities such as Al and P to generate carriers. Si_xGe_{1-x} alloys enable band tuning in that the composition x can be changed continuously to control the energy band gap.^{1,2} This advantage leads to another beneficial feature, namely, a Si/Si_xGe_{1-x}/Si superlattice, where the band offsets at the heterointerface are effectively adopted for charge transfer and confinement. Such fine processes for blending heteromaterials, even at the atomic level, permit silicon to be utilized in a wide range of applications. How about organic semiconductors? Considerable effort has been devoted to developing various organic electronic devices, including transistors, solar cells, and light-emitting devices.^{3–7} Organic semiconductors have certain advantages with respect to realizing large area devices on flexible substrates in low-cost processes.⁸ In contrast to such application-oriented studies, we still need to obtain a fundamental understanding if we are to establish fine processes, particularly those for constructing heteromaterials. If we can establish such processes for assembling heteromolecules, e.g., molecular doping, molecular alloying, and molecular superlattice, the full potential of the diverse range of organic molecules can be realized. For this purpose, we have examined solid-state reactions in binary molecular assemblies to

ABSTRACT Various phases of binary molecular assemblies of perfluorinated Cu-phthalocyanine (F₁₆CuPc) and pentacene were examined using scanning tunneling microscopy (STM). Alloying, solid solutions, phase separation, and segregation were observed in assemblies on monolayers according to the mixture ratios. The main driving force behind such molecular blending is CH–F hydrogen bonds. Lattice matching and molecular symmetry are other factors that determine the assembly configuration. A detailed understanding of such solid-state reactions provides a guideline to the construction of multilayered binary assemblies, where intermixing between molecules takes place when multiple layers are stacked.

KEYWORDS: scanning tunneling microscopy • self-assembly • hydrogen bonds • molecular alloy • molecular solid solution

obtain insight into the basic mechanism of heteromolecule assembly.

Over the past few years, multimolecular assemblies have been studied on the basis of STM. The self-assembly features of molecules can generate various configurations including porous molecular networks,^{9–11} guest–host systems,^{12,13} and charge transfer complexes.^{14,15} Some combinations of heteromolecules produce different phases depending on the mixture ratios,^{16–18} which can in turn be employed to arrange the intervals of specific molecules with spacers.^{19–21} As a result, organic molecules have potential as functional building blocks, and STM contributes greatly in terms of providing detailed analyses.

We employed pentacene and F₁₆CuPc in this study. Here, the strong electron affinity of fluorine atoms attached to the phthalocyanine plays a key role. First, the HOMO–LUMO levels of F₁₆CuPc are lowered to deep levels because of the electron-withdrawing property of the F atoms.^{22,23} As a result, F₁₆CuPc can function as an n-type semiconductor. In contrast most organic semiconductors exhibit p-type properties. Therefore, a pentacene–F₁₆CuPc pair

*Address correspondence to wakayama.yutaka@nims.go.jp.

Received for review October 13, 2010 and accepted December 03, 2010.

Published online December 13, 2010. 10.1021/nn102887x

© 2011 American Chemical Society

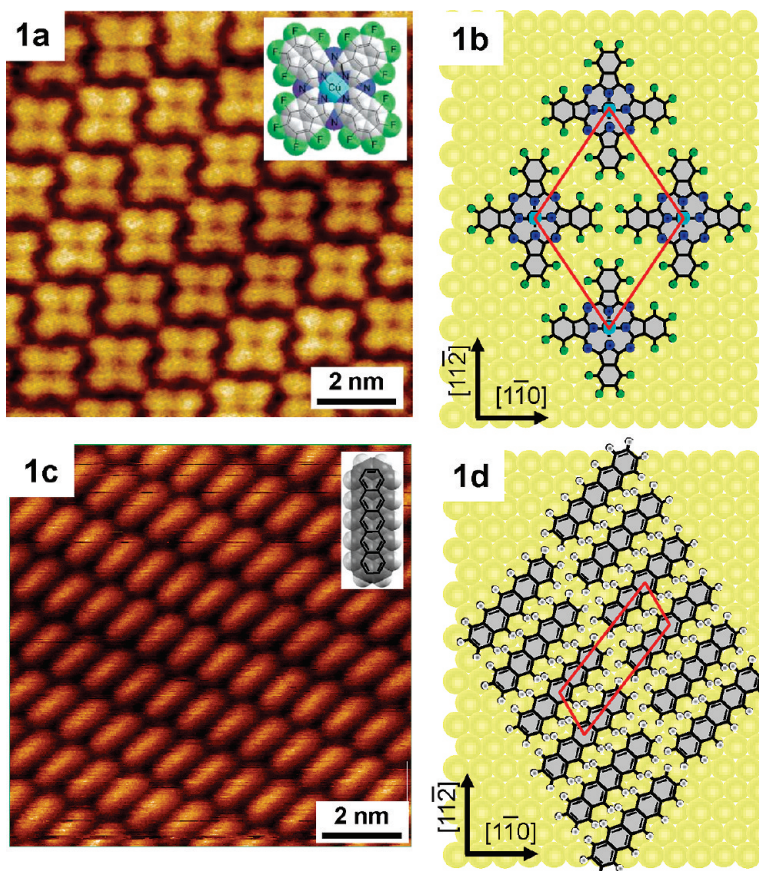


Figure 1. STM images of $F_{16}\text{CuPc}$ and pentacene monolayers and their unit cells showing the crystallographic relationship with Au(111).

can be regarded as a molecular p–n junction or can work as a donor–acceptor pair.²⁴ Second, the fluorine atoms form hydrogen bonds (CH–F bonds), which generate an attractive force with neighboring pentacene.^{18,21,25–27} For these reasons, we adopted pentacene– $F_{16}\text{CuPc}$ molecules and examined their molecular arrangements on monolayer and multilayer assemblies using STM.

RESULTS AND DISCUSSION

Crystalline Phases in Monolayers. Figure 1 shows STM images of $F_{16}\text{CuPc}$ and pentacene monolayers. $F_{16}\text{CuPc}$ forms a rhombic unit cell with a lattice constant of approximately 1.5 nm. The diagonals of $F_{16}\text{CuPc}$ are along the $[1\bar{1}2]$ and $[1\bar{1}0]$ axes^{28,29} (see Figure 1a and b) of the Au(111) surface. The STM image in Figure 1c shows a typical assembly of pentacene with one monolayer. The lattice constants are approximately 0.6 and 1.5 nm. The long axis of pentacene rotated slightly with respect to the $[1\bar{1}0]$ directions of the Au surface. As France *et al.* have reported,³⁰ pentacene on Au(111) exhibits various types of polymorphism; the azimuthal orientations and lattice constants can be changed depending on the coverage. The observed pure pentacene phase in Figure 1c is one example of this polymorphism, which corresponds to the type-C structure in France's report. This flexibility of the molecular alignment of

pentacene allows us to realize a variety of layouts in binary assemblies as discussed later.

The co-deposition of these molecules achieves a well-mixed phase formation and molecular arrangements that depend on the ratios. Figure 2a shows STM images of the 1:1 phase and an illustration of the unit cell. The same quantities of molecules supplied to the surface simultaneously resulted in an alternating arrangement of the molecules. The long axis of pentacene and one of the diagonals of $F_{16}\text{CuPc}$ were aligned along the $[1\bar{1}0]$ direction of the Au(111) surface. This kind of mixed phase can be formed at different ratios. Figure 2b shows an STM image of the 2:1 phase. The molecular ratios are henceforth represented by the pentacene: $F_{16}\text{CuPc}$ ratio. The pentacene dimer and $F_{16}\text{CuPc}$ monomer are aligned to form the unit cell. This phase has a porous molecular network, and the density of the molecules is less than that of the 1:1 phase. The similarity of the 1:1 and 2:1 phases lies in the orientation of $F_{16}\text{CuPc}$; the diagonals of $F_{16}\text{CuPc}$ in both phases coincide with those in the pure $F_{16}\text{CuPc}$ phase. Meanwhile, both molecules have unique orientations in the 2:1 phase, unlike the zigzag alignment in the 1:1 phase. Figure 2c shows an STM image of the 3:1 phase. $F_{16}\text{CuPc}$ molecules are distributed in a regular manner between pentacene trimers. The molecular alignment in rows (indicated by arrows in Figure 2c) is common for the pure pentacene phase (Figure 1b), and the pentacene orientation is also almost the same as that observed in Figure 1b. However, the interval between neighboring pentacene molecules (about 0.8 nm) is more than 30% larger than that of the pure pentacene phase.

The hydrogen bonds (H-bonds) between the fluorine atoms of $F_{16}\text{CuPc}$ and the hydrogen atoms of pentacene constitute the main driving force behind mixed phase formation. Figure 3a–c shows the molecular alignment of the respective phases (1:1, 2:1, and 3:1). Here, the H-bonds with an F–H distance of less than 3.0 Å are indicated by red dotted lines. There are 20, 16, and 14 H-bonds in the respective phases. The energetic gains realized by forming H-bonds are estimated by the DFT calculation. We found that the energies normalized by the area were clearly proportional to the H-bond density as shown in Figure 3d. The 1:1 phase was the most stable due to the highly extended H-bonded network. Meanwhile, the 3:1 phase showed a relatively smaller gain. This is because the pentacene molecule at the trimer center (labeled “c” in Figure 2c) had no H-bonds with the adjacent $F_{16}\text{CuPc}$ molecules (“t” and “b”). The wide intermolecular intervals observed in Figure 2c can also be explained by such an H-bonded network. The pentacene molecules on both sides in

the trimers are drawn by the intense H-bonds with neighboring F₁₆CuPc ("l" and "l"). This is naturally much stronger than the van der Waals interaction with pentacene ("c") on the other side, resulting in the larger lattice constant in the pentacene trimer.

The crystalline phases can be formed only at certain ratios of pentacene to F₁₆CuPc (1:1, 2:1, and 3:1). This is comparable to the "alloying" commonly observed in inorganic materials, *e.g.*, Ni silicides such as Si₂Ni, SiNi, and SiN₂ on a Si substrate.³¹ In such cases, important roles are played by the accommodation of a lattice constant and the attractive force between components as well as the symmetry of the constituent elements, which are essential factors common to both inorganic and organic materials.

Solid Solution, Phase Separation, and Segregation. The minimum composition of F₁₆CuPc needed to form the crystalline phase was 25% (3:1 ratio). A further decrease in the concentration resulted in the random distribution of F₁₆CuPc in the pentacene matrix. Figure 4a shows an STM image of a mixed layer with diluted F₁₆CuPc molecules whose concentration is about 11% (8:1 ratio). The basic molecular alignment is similar to that of the pure pentacene phase. The dotted circles in the STM image represent the random distribution of F₁₆CuPc. The enlarged image in Figure 4b emphasizes the local molecular arrangement, which is the same as that of the 3:1 phase. One F₁₆CuPc molecule is surrounded by eight pentacene molecules, as illustrated in the figure, where the H-bonded network is responsible for stabilizing heteromolecule blending in a local area.

This mixed phase can be regarded as a "solid solution", which is well known in inorganic semiconductors such as Ga_xAl_{1-x}As and Si_xGe_{1-x}. The F₁₆CuPc concentration "*x*" can be changed continuously in the 0.00–0.25 range in the compositional formula of {F₁₆CuPc}_x{pentacene}_{1-x}. Then the pure pentacene phase can be doped with even a small amount of F₁₆CuPc in a similar manner to the impurity doping of Si crystals with P and Al. Here, the width of F₁₆CuPc is approximately 1.5 nm, which is comparable to the size of pentacene. Such equivalence of the molecular sizes, in other words lattice matching, enables us to achieve heteromolecule doping without disordering the original pentacene alignment. In fact, the solid solution was a unique assembly observed only in the pentacene–F₁₆CuPc binary system. We did not observe it in other molecular combinations, *e.g.*, the tetracene–F₁₆CuPc and coronene–F₁₆CuPc binary systems. Both tetracene and coronene are benzenoid aromatic compounds similar to pentacene that can form H-bonds with F₁₆CuPc. However, the mixtures of these molecules with F₁₆CuPc showed only crystalline phases at certain ratios and no solid solution was observed at any ratio. This is because the mismatch in size and symmetry prevents the formation of a solid solution with F₁₆CuPc (see Supporting Information).

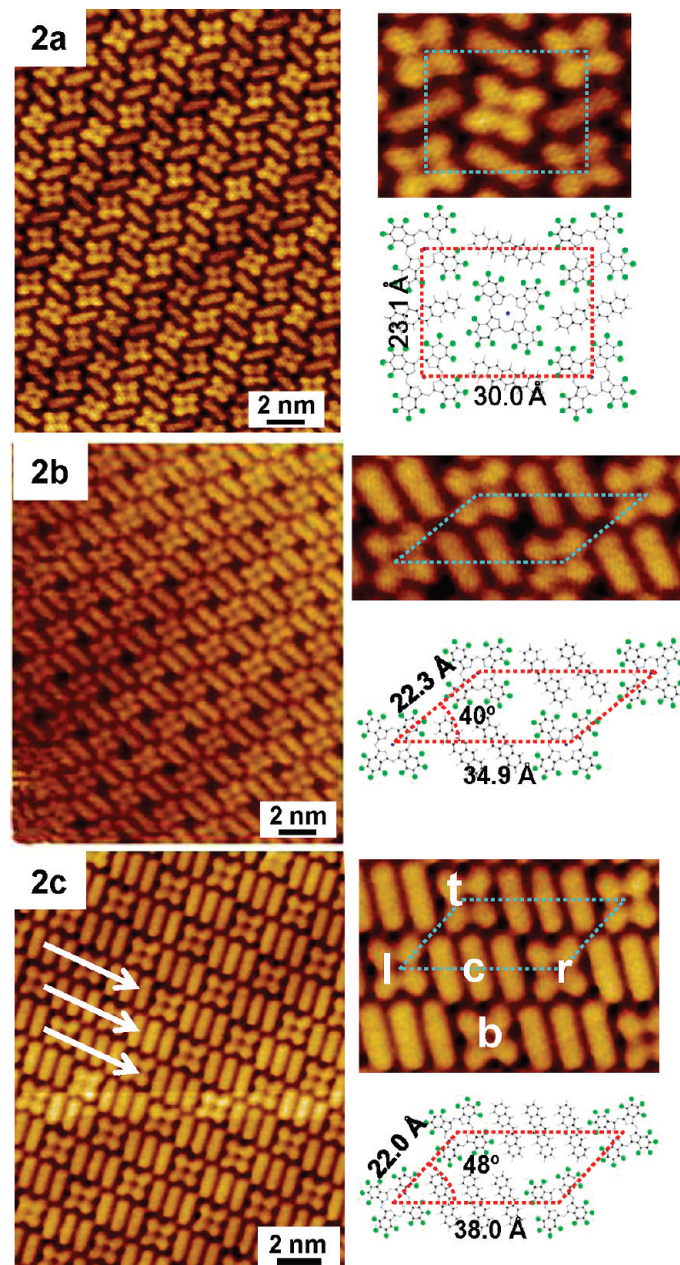


Figure 2. STM images of wide and magnified areas and illustrations showing lattice parameters for different mixture ratios. (a) 1:1 phase. Respective molecules are aligned alternately with a zigzag orientation. (b) 2:1 phase. Pentacene dimers and F₁₆CuPc monomers are aligned alternately to form a unit cell. (c) 3:1 phase. Pentacene trimers and F₁₆CuPc monomers are aligned alternately to form a unit cell. The molecules were assembled in rows as indicated by the arrows in a similar manner to pentacene assembly. Pentacene at the trimer center and surrounding four F₁₆CuPc were labeled c, t, b, l, and r, according to their locations.

In contrast, no specific phase or solid solution was formed for a F₁₆CuPc-rich composition higher than 50%. Phase separation was clearly observed between the 1:1 phase and the pure F₁₆CuPc phase, as shown in Figure 5a. Each phase formed domains several tens of nanometers in size. The STM image in Figure 5b demonstrates that the respective phases can be divided from each other with a distinct boundary, as shown by the dashed line. These results can be attributed to the

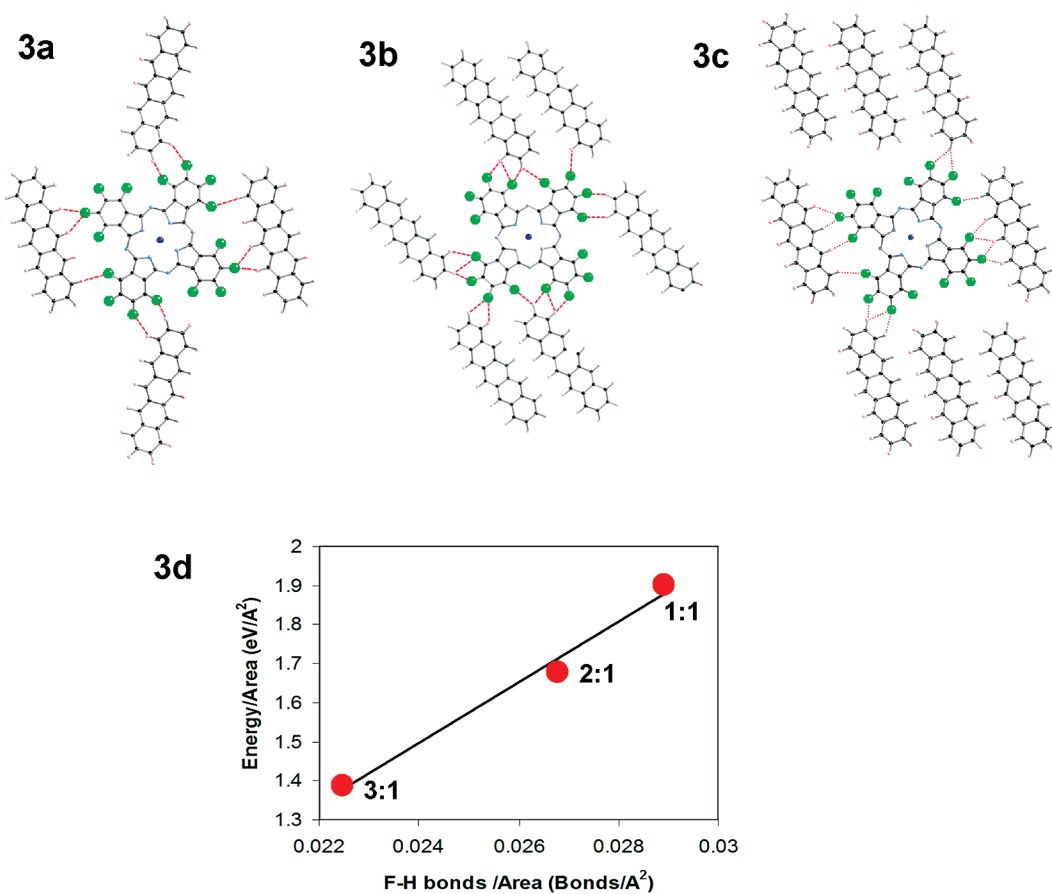


Figure 3. Hydrogen-bonding networks of (a) 1:1 phase, (b) 2:1 phase, and (c) 3:1 phase, obtained with the DFT calculation. The hydrogen bonds, whose F–H distances are less than 3.0 Å, are shown by red dotted lines. (d) Energetic gains with the hydrogen bonds of respective phases. Energies normalized by area are proportional to the hydrogen-bonding density.

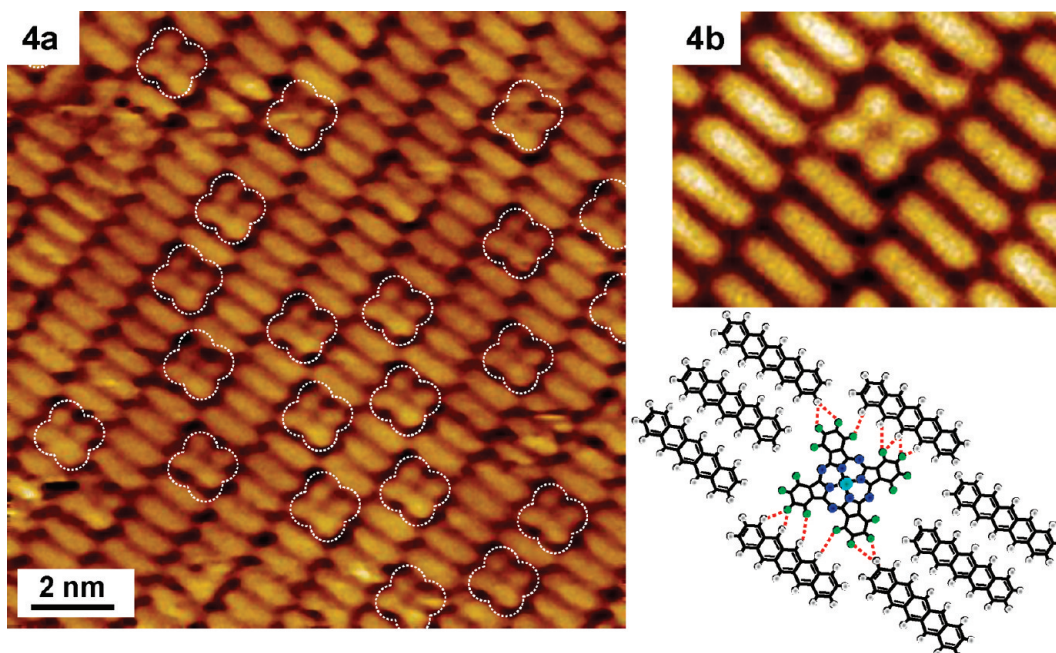


Figure 4. (a) STM image of the pentacene-rich mixture with a F₁₆CuPc concentration of 11%. F₁₆CuPc molecules, shown by the dotted circles, are distributed randomly in the pentacene matrix. (b) The enlarged image indicates that the F₁₆CuPc molecules are surrounded by pentacene in a similar manner to the 3:1 phase. The expected H-bonds are shown. The H-bonded network stabilizes the incorporation of heterogeneous molecules into the pentacene lattice.

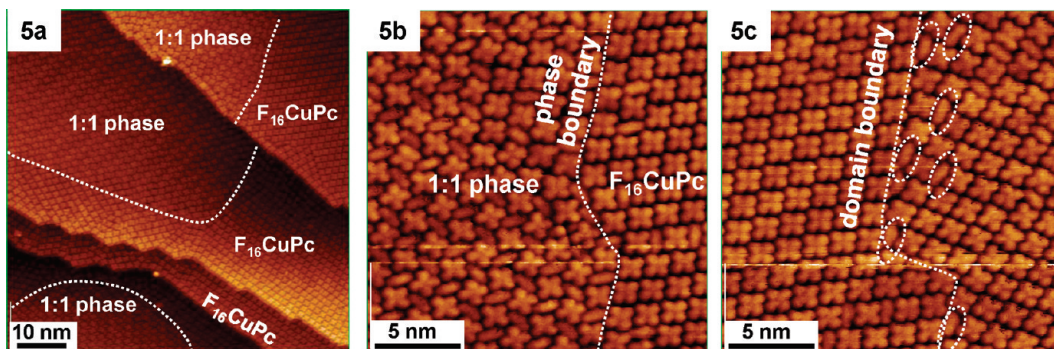


Figure 5. STM images of $F_{16}\text{CuPc}$ -rich mixtures. The phase boundaries between pure $F_{16}\text{CuPc}$ and 1:1 phase are shown by dashed lines. (a) A wide range image clarifies the phase separation between $F_{16}\text{CuPc}$ and the 1:1 phase. (b) The magnified image emphasizes the phase boundary. (c) The pentacene molecules in the $F_{16}\text{CuPc}$ matrix are segregated around the grain boundary, as emphasized by the ellipses.

high stability of the 1:1 phase as clarified by the calculation. No other stable molecular configurations can be formed in a $F_{16}\text{CuPc}$ -rich composition. However, to be exact, a minute amount of pentacene can be incorporated in the $F_{16}\text{CuPc}$ phase, as indicated by the dotted ellipses in Figure 5c. These molecules tend to appear in the vicinity of domain boundaries (dashed line in Figure 5c). Postannealing made this tendency more pronounced. Therefore, it is reasonable to conclude that pentacene molecules are segregated and cannot be blended into the $F_{16}\text{CuPc}$ phase.

These experimental data are summarized in the phase diagram in Figure 6. Various solid-state reactions, including alloying, solid solution, molecular doping, phase separation, and segregation occurred in the monolayer molecular assemblies. The unique orientation of $F_{16}\text{CuPc}$ was commonly observed in all phases. Meanwhile, pentacene showed flexibility as regards the lattice parameters,^{30,32} which enabled it to accommodate different molecular arrangements and form a wide range of mixed phases depending on the mixture ratios.

Multiple Layers. Alternating deposition was carried out to examine multiple heterolayer stacking. First, monolayers of each molecule were deposited, followed

by the subsequent deposition of their counterparts. In Figure 7a and b, additional $F_{16}\text{CuPc}$ was deposited as the second layer on the first pentacene monolayer. Although we expected $F_{16}\text{CuPc}$ simply to stack on the pentacene, the experimental results revealed the formation of complex mixtures. The $F_{16}\text{CuPc}$ molecules were incorporated in the pentacene lattice. The enlarged image in Figure 7b clearly reveals that the molecular arrangement is the same as that of the solid solution produced by the co-deposition shown in Figure 4. Interestingly, some pentacene molecules can be seen as a second layer with a dark contrast as indicated by the arrows in Figure 7a. As reported previously, the pentacene molecules on the first monolayer aggregate to form one-dimensional rows.³⁰ We assume that these molecules were originally located in the pentacene matrix, but were later ejected by the $F_{16}\text{CuPc}$ molecules. The molecular arrangement in a local area, where one $F_{16}\text{CuPc}$ is surrounded by eight pentacene molecules, is the same as that of the 3:1 phase in Figure 2c. Therefore, we consider that the pentacene molecules were ejected to gain energy of $1.4\text{ eV}/\text{\AA}^2$ by forming H-bonds, as discussed in Figure 3c and d. Careful observation clarified that the linear alignment of the pentacene lattice in the first monolayer involves a slight fluctuation

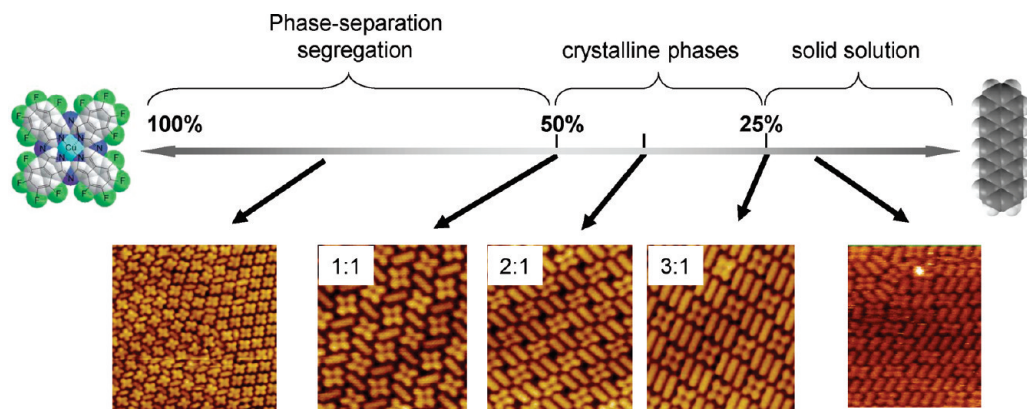


Figure 6. Phase diagram of the $F_{16}\text{CuPc}$ -pentacene binary system. Crystalline phases can be formed only at ratios of 3:1, 2:1, and 1:1. More than 50% of $F_{16}\text{CuPc}$ results in phase separation and segregation. A diluted $F_{16}\text{CuPc}$ concentration of less than 25% causes the formation of a solid solution. The concentration of $F_{16}\text{CuPc}$ can be changed continuously in the 0–25% range, where the $F_{16}\text{CuPc}$ molecules are distributed randomly in the pentacene matrix.

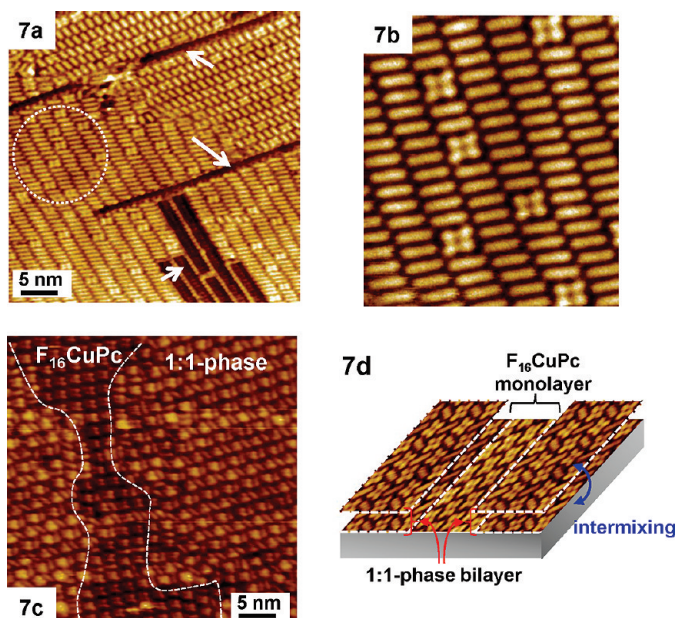


Figure 7. STM images of multiple layers. (a) F₁₆CuPc molecules deposited on the first pentacene monolayer were incorporated into the pentacene matrix. The pentacene molecules originally seated in the matrix were pushed out to form pentacene rows as the second layer (see the arrows). The alignment of the pentacene molecules in the encircled area involved fluctuation, which was assumed to be induced by the hydrogen bonds with neighboring F₁₆CuPc. (b) The enlarged STM image shows the formation of a solid solution produced by the sequential deposition of F₁₆CuPc after pentacene. (c, d) STM image and schematic illustration of the multilayer, where the pentacene molecules were deposited on the first F₁₆CuPc monolayer. Intermixing occurred with the pentacene deposition to form a 1:1 phase bilayer, leaving the original F₁₆CuPc monolayer.

(see the molecules in the dotted circle in Figure 7a). This is probably induced by the F₁₆CuPc molecules, which exhibit an attractive interaction through the H-bonds with the surrounding pentacene molecules.

Figure 7c shows an STM image, where the molecules were deposited in reverse sequence. F₁₆CuPc was deposited as the first layer, followed by pentacene. In this case, 1:1 phase domains were observed on both sides of the image, leaving the original F₁₆CuPc monolayer around the center region. The height profile indicated that the 1:1 phase domains consisted of double layers. That is, the intermixing between the molecules in the first and second layers occurred with pentacene deposition to form a 1:1 phase bilayer, as shown schematically in Figure 7d.

The intermixing observed here and the solid solution in Figure 7a correspond well with the results summarized in the phase diagram. Namely, the coexistence of the 1:1 phase bilayer and the F₁₆CuPc monolayer is essentially equivalent to the phase separation observed with a F₁₆CuPc-rich concentration. Meanwhile, even a small amount of F₁₆CuPc can be dissolved in the pentacene to form a solid solution with a pentacene-rich concentration. These phenomena suggest that the energetic gain obtained by H-bonds in the lateral direction has a dominant effect in terms of stabilizing the total molecular arrangement. These experimental results

make it clear that the first layer should be sufficiently stable to avoid molecular mixing and to serve as a platform for the second layer.

We chose the 1:1 phase as the first monolayer because the molecules adopt an alternating arrangement to produce a stable phase with a complex H-bonded network. The respective molecules were subsequently deposited on the 1:1 phase as shown in Figure 8. Figure 8b is an STM image, where one monolayer of F₁₆CuPc was deposited on the first 1:1 monolayer. The molecular orientation cannot be identified because of the poor resolution of the image. However, the periodicity observed here coincides well with that of the pure F₁₆CuPc phase in Figure 1a. The configuration of this heterodouble layer, *i.e.*, F₁₆CuPc on 1:1, is essentially the same as that of the phase separation observed in Figure 5. The difference is simply the direction of the phase separation, namely, the lateral separation in Figure 5 and the vertical separation in Figure 8b. On the basis of these results, we conclude that (1:1)-(F₁₆CuPc) multiple stacking can be realized with sufficient stability.

In contrast, pentacene deposition on the 1:1 phase exhibited complexity as shown in Figure 8c and d. Here, a small amount of pentacene that was less than a monolayer was deposited on the first 1:1 monolayer. Although part of the deposited pentacene can be seen as dark lines in the second layer (see the arrow in Figure 8c), most of the pentacene molecules began mixing with the first 1:1 layer. The STM image was recorded several minutes after the deposition, and the original 1:1 phase was never observed. Therefore, it is reasonable to consider that the mixing started almost concurrently with the deposition. The molecules in the dotted circle in Figure 8c have a random arrangement, which is evidence of mixing. However, interestingly enough, another STM image obtained about 4 min later revealed that these mixed molecules rearranged themselves into the 3:1 phase as shown by the circle in Figure 8d. These experimental results suggest that the 3:1 phase is also stable, which contrasts with our results. A possible reason is that the Au(111) surface helps determine the most stable alignment of the first layer. However, the details remain a subject for further study.

In accordance with these experimental results, we adopted the 3:1 phase as the first layer. The 3:1 phase layers on the Au(111) were covered by second layers consisting of F₁₆CuPc (Figure 9a) and pentacene (Figure 9b), respectively. The submonolayer deposition of each molecule induced the formation of islands. These islands were confirmed to be stable and no intermixing was observed. The F₁₆CuPc molecules were aligned in rows with a tilting angle of about 60°, which was distinct from the two-dimensional array with a flat orientation in the 1:1 phase shown in Figure 8b. Such a one-dimensional alignment in the second layers is commonly observed for pentacene as shown in Figure 9b and also in Figures 7a, 8c, and 8d. The growth direc-

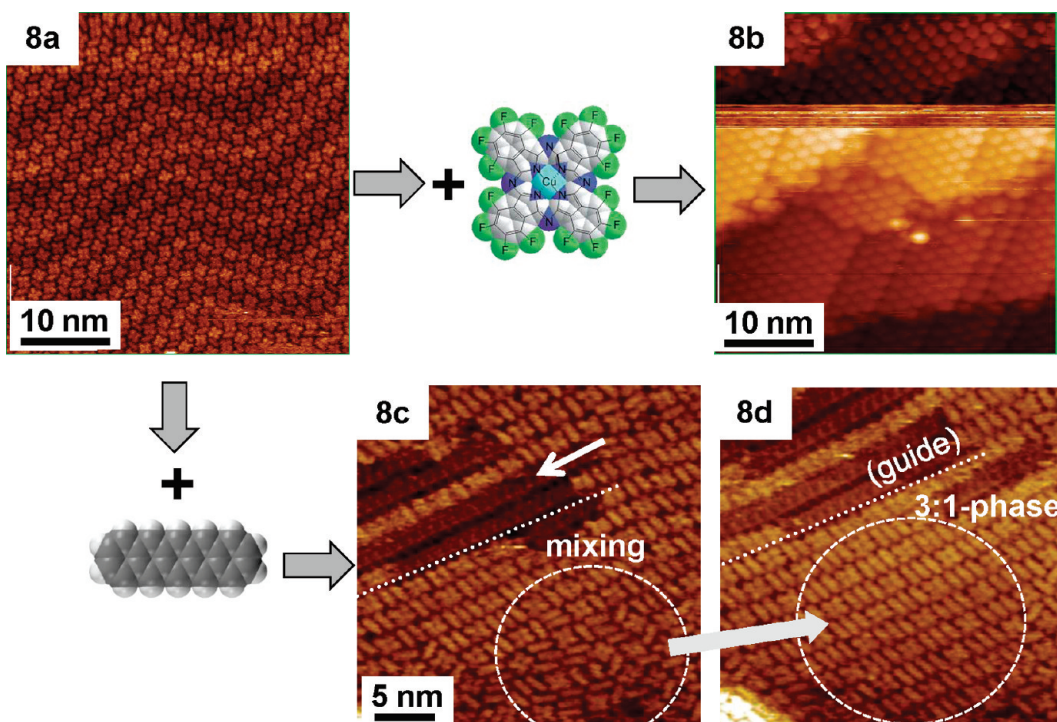


Figure 8. STM images of (a) a 1:1 phase serving as the first layer and (b) a F₁₆CuPc monolayer formed on the 1:1 phase. (c) Subsequent deposition of pentacene on the 1:1 phase induced mixing and rearrangement of the molecules. Some molecules exhibited disordering as shown by the dotted circle, while some other pentacene molecules formed rows as the second layers (see arrow). (d) Several minutes later, the molecules in the first layer were rearranged into the 3:1 phase, suggesting that this phase is also stable.

tion of the 1D rows in the first layer is copied in the second layer. The high-resolution image in Figure 9b revealed that the pentacene in the second layer (drawn in red) involved an azimuthal rotation of 25° with re-

spect to that of the first layer. This rotational mismatch is probably induced to avoid a repulsive π-electron interaction between stacked pentacene molecules. Moreover, the interval of the neighboring pentacene in the

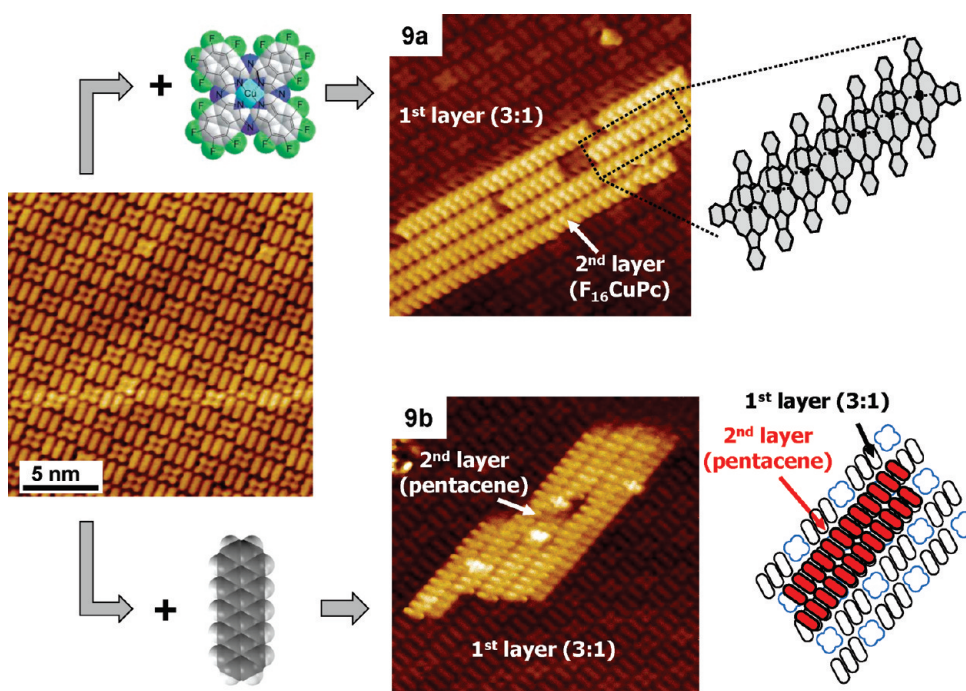


Figure 9. STM images of (a) F₁₆CuPc and (b) pentacene on the 3:1 phase. Both molecules formed stable islands without any mixing or rearrangement. F₁₆CuPc and pentacene aligned in rows reflecting the alignment of the first layer with the tilting angle and rotating mismatch, respectively.

second layer was about 13% smaller than that of the pentacene in the underlying 3:1 phase. These results indicate that the molecular arrangements in the second layer, including the growth direction, azimuthal orientation, and lattice constant, are affected by those in the first layer.

CONCLUSION

In summary, various solid-state reactions between F₁₆CuPc and pentacene were analyzed by employing STM observations. First, the monolayer assemblies were investigated to obtain a fundamental insight into the growth mechanism of heteromolecule assemblies. Crystalline phases, solid solutions, and phase separation were observed depending on the blending ratios. The hydrogen bonds are mainly responsible for the mixtures. The size and symmetry of the molecules play additional but essential roles in producing various assem-

blies. These findings summarized in the phase diagram are valid when stacking multilayers. When the total concentration of pentacene exceeds 75%, i.e., in the solid solution range, intermixing and rearrangement take place, which disturb simple multilayer stacking. In contrast, a F₁₆CuPc concentration exceeding 50% resulted in phase separation, thus enabling the stacking of stable heterolayers. Otherwise, the underlying first layer should be sufficiently stable, as with the 3:1 phase, to serve as the platform for subsequent layers. In other words, a well-chosen sequence of stacking layers makes it possible to produce artificial organic thin films with various compositions and molecular orientations. These detailed discussions of solid-state reactions in molecules mark an important first step toward the band engineering and crystal engineering of organic semiconductors.

EXPERIMENTAL SECTION

All experimental procedures, including substrate cleaning, molecular deposition, and STM observation, were performed in an ultrahigh vacuum with a background pressure of 1×10^{-8} Pa. A single-crystal Au(111) surface was used as a substrate. An atomically clean surface was obtained by employing cycles of Ar⁺ ion sputtering and thermal annealing at 600 K and was confirmed by the clear observation of a reconstructed herringbone pattern on Au(111). The substrate was kept at room temperature during molecular deposition. Both the F₁₆CuPc and pentacene molecules were deposited from Knudsen cells at a rate of about 0.1 monolayer (ML)/min. The opening and closing times of the shutters were adjusted during co-deposition to tune the composition ratios. STM observation was carried out at room temperature. The tunneling currents and bias voltages were typically 50–70 pA and 60–80 mV, respectively. Energies obtained by forming hydrogen bonds were estimated using a theoretical calculation based on density functional theory (DFT). The DFT calculations were performed with the GPAW code³³ using periodic boundary conditions. The exchange–correlation energy was calculated according to the van der Waals (vdW)-DFT functional proposed by Dion *et al.*³⁴ This functional is explicitly constructed to include nonlocal dispersion interactions, which are expected to be significant here. Due to the sizes of the systems, the Au(111) substrate was not taken into account in the calculations, except for an imposed planarity requirement for the resulting structures.

Supporting Information Available: STM images of tetracene–F₁₆CuPc and coronene–F₁₆CuPc binary systems as evidence for the absence of a solid solution. This material is available free of charge via the Internet at <http://pubs.acs.org>.

REFERENCES AND NOTES

- Wakahara, A.; Kuramoto, K.; Hasegawa, T.; Noda, S.; Sasaki, A. Photoluminescence Processes in Si_{1-x}Ge_x/Si Disordered Superlattices Grown on Si(001) Substrate. *J. Appl. Phys.* **1997**, *82*, 392–396.
- Presting, H.; Kibbel, H.; Jaros, M.; Turton, R. M.; Menczigar, U.; Abstreiter, G.; Grimmel, H. G. Ultrathin SiGe Strained Layer Superlattices—A Step towards Si Optoelectronics. *Semicond. Sci. Technol.* **1992**, *7*, 1127–1148.
- Yamashita, Y. Organic Semiconductors for Organic Field-Effect Transistors. *Sci. Technol. Adv. Mater.* **2009**, *10*, 024313–024321.
- Dodabalapur, A. Organic and Polymer Transistors for Electronics. *Mater. Today* **2006**, *9*, 24–30.
- Heremans, P.; Cheyns, D.; Rand, B. P. Organic Solar Cells: Material Selection and Device Architecture. *Acc. Chem. Res.* **2009**, *42*, 1740–1747.
- Helgesen, M.; Søndergaard, R.; Krebs, F. C. Advanced Materials and Processes for Polymer Solar Cell Devices. *J. Mater. Chem.* **2010**, *20*, 36–60.
- Samuel, I. D. W.; Turnbull, G. A. O. Organic Semiconductor Laser. *Chem. Rev.* **2007**, *107*, 1272–1295.
- Forrest, S. R. The Path to Ubiquitous and Low-Cost Organic Electronic Appliances on Plastic. *Nature* **2004**, *428*, 911–918.
- Swarbrick, J. C.; Rogers, B. L.; Champness, N. R.; Beton, P. H. Hydrogen-Bonded PTCDA-Melamine Networks and Mixed Phases. *J. Phys. Chem. B* **2006**, *110*, 6110–6114.
- Theobald, J. A.; Oxtoby, N. S.; Phillips, M. A.; Champness, N. R.; Beton, P. H. Controlling Molecular Deposition and Layer Structure with Supramolecular Surface Assemblies. *Nature* **2003**, *424*, 1029–1031.
- Stöhr, M.; Wahl, M.; Spillmann, H.; Gade, L. H.; Jung, T. A. Lateral Manipulation for the Positioning of Molecular Guests within the Confinements of a Highly Stable Self-Assembled Organic Surface Network. *Small* **2007**, *3*, 1336–1340.
- Mena-Osteritz, E.; Bäuerle, P. Complexation of C₆₀ and Cyclo thiophene Monolayer Template. *Adv. Mater.* **2006**, *18*, 447–451.
- Kiebele, A.; Bonifazi, D.; Cheng, F.; Stöhr, M.; Diederich, F.; Jung, T. A.; Spillmann, H. Adsorption and Dynamics of Long-Range Interacting Fullerenes in a Flexible, Two-Dimensional, Nanoporous Porphyrin Network. *ChemPhysChem* **2006**, *7*, 1462–1470.
- Jäckel, F.; Perera, U. G. E.; Iancu, V.; Braun, K.-F.; Koch, N.; Rabe, J. P.; Hla, S.-W. Investigating Molecular Charge Transfer Complexes with a Low Temperature Scanning Tunneling Microscope. *Phys. Rev. Lett.* **2008**, *100*, 126102–126105.
- Samuely, T.; Liu, S.-X.; Haas, M.; Decurtins, S.; Jung, T. A.; Stöhr, M. Self-assembly of Individually Addressable Complexes of C₆₀ and Phthalocyanines on a Metal Surface: Structural and Electronic Investigations. *J. Phys. Chem. C* **2009**, *113*, 19373–19375.
- Bobisch, C.; Wagner, Th.; Bannani, A.; Möller, R. Ordered Binary Monolayer Composed of Two Organic Molecules: Copper-Phthalocyanine and 3,4,9,10-perylene-tetra-carboxylic-dianhydride on Cu(111). *J. Chem. Phys.* **2003**, *119*, 9804–9808.
- de Wild, M.; Berner, S.; Suzuki, H.; Yanagi, H.; Schlettwein,

- D.; Ivan, S.; Baratoff, A.; Guentherodt, H.-J.; Jung, T. A. A Novel Route to Molecular Self-Assembly: Self-Intermixed Monolayer Phases. *ChemPhysChem* **2002**, *3*, 881–885.
18. Barrena, E. G.; de Oteyza, D.; Dosch, H.; Wakayama, Y. 2D Supramolecular Self-Assembly of Binary Organic Monolayers. *ChemPhysChem* **2007**, *8*, 1915–1918.
19. Treier, M.; Nguyen, M.-T.; Richardson, N. V.; Pignedoli, C.; Passerone, D.; Fasel, R. Tailoring Low-Dimensional Organic Semiconductor Nanostructures. *Nano Lett.* **2009**, *9*, 126–131.
20. Xu, B.; Tao, C.; Williams, E. D.; Reutt-Robey, J. E. Coverage Dependent Supramolecular Structures: C_{60} : ACA Monolayers on Ag(111). *J. Am. Chem. Soc.* **2006**, *128*, 8493–8499.
21. Huang, Y. L.; Chen, W.; Li, H.; Ma, J.; Pflaum, J.; Wee, A. T. S. Tunable Two-Dimensional Binary Molecular Networks. *Small* **2010**, *6*, 70–75.
22. G. de Oteyza, D.; Silanes, I.; Ruiz-Ose's, M.; Barrena, E.; Doyle, B. P.; Arnau, A.; Dosch, H.; Wakayama, Y.; Ortega, J. E. Balancing Intermolecular and Molecule-Substrate Interactions in Supramolecular Assemblies. *Adv. Funct. Mater.* **2009**, *19*, 259–264.
23. Shen, C.; Kahn, A. Electronic Structure, Diffusion, and p-doping at the Au/ $F_{16}CuPc$ Interface. *J. Appl. Phys.* **2001**, *90*, 4549–4554.
24. G. de Oteyza, D.; Garcíá-Lastra, J. M.; Corso, M.; Doyle, B. P.; Floreano, L.; Morgante, A.; Wakayama, Y.; Rubio, A.; Ortega, J. E. Customized Electronic Coupling in Self-Assembled Donor-Acceptor Nanostructures. *Adv. Funct. Mater.* **2009**, *19*, 3567–3573.
25. Huang, Y. L.; Li, H.; Ma, J.; Huang, H.; Chen, W.; Wee, A. T. S. Scanning Tunneling Microscopy Investigation of Self-Assembled CuPc/ $F_{16}CuPc$ Binary Superstructures on Graphite. *Langmuir* **2010**, *26*, 3329–3334.
26. Krauss, T. N.; Barrena, E.; Dosch, H.; Wakayama, Y. Supramolecular Assembly of a 2D Binary Network of Pentacene and Phthalocyanine on Cu(100). *ChemPhysChem* **2009**, *10*, 2445–2448.
27. Hovanessian, A. D.; Doyon, J. B.; Jain, A.; Rablen, P. R.; Sapce, A.-M. Models of F·H Contacts Relevant to the Binding of Fluoroaromatic Inhibitors to Carbonic Anhydrase II. *Org. Lett.* **1999**, *1*, 1359–1362.
28. Huang, H.; Chen, W.; Wee, A. T. S. Low-Temperature Scanning Tunneling Microscopy Investigation of Epitaxial Growth of $F_{16}CuPc$ Thin Films on Ag(111). *J. Phys. Chem. C* **2008**, *112*, 14913–14918.
29. Wakayama, Y. Assembly Process and Epitaxy of the $F_{16}CuPc$ Monolayer on Cu(111). *J. Phys. Chem. C* **2007**, *111*, 2675–2678.
30. France, C. B.; Schroeder, P. G.; Forsythe, J. C.; Parkinson, B. A. Scanning Tunneling Microscopy Study of the Coverage-Dependent Structures of Pentacene on Au(111). *Langmuir* **2003**, *19*, 1274–1281.
31. Mattieis, R.; Hesse, D. A Reinvestigation of Ni, Si Thin Film Growth on Si(111) by TEM and RBS. *Phys. Status Solidi A* **1988**, *109*, 217–229.
32. Müller, K.; Kara, A.; Kim, T. K.; Bertschinger, R.; Scheybal, A.; Osterwalder, J.; Jung, T. A. Multimorphism in Molecular Monolayers: Pentacene on Cu(110). *Phys. Rev. B* **2009**, *79*, 245421–245427.
33. Enkovaara, J.; Rostgaard, C.; Mortensen, J. J.; Chen, J.; Dulák, M.; Ferrighi, L.; Gavnholz, J.; Glinsvad, C.; Haikola, V.; Hansen, H. A.; et al. Electronic Structure Calculations with GPAW: A Real-Space Implementation of the Projector Augmented-Wave Method. *J. Phys.: Condens. Matter* **2010**, *22*, 253202.
34. Dion, M.; Rydberg, H.; Schroder, E.; Langreth, D. C.; Lundqvist, B. I. Density Functional for General Geometries. *Phys. Rev. Lett.* **2004**, *92*, 246401_1–246401_4.